A theory for the pressure pedestal in high (H) mode tokamak discharges

P. N. Guzdar
Institute for Research in Electronics and Applied Physics, University of Maryland, College Park, Maryland 20742

S. M. Mahajan
Institute for Fusion Studies, University of Texas, Austin, Texas 78712

Z. Yoshida
Faculty of Engineering, University of Tokyo, Hongo, Tokyo 113, Japan

(Received 30 August 2004; accepted 6 December 2004; published online 8 February 2005)

When a tokamak plasma makes a transition into the good or the high confinement H mode, the edge density and pressure steepen and develop a very sharp pressure pedestal. Prediction of the height and width of this pressure profile has been actively pursued so as to provide a reliable extrapolation to future burning plasma devices. The double-Beltrami two-fluid equilibria of Mahajan and Yoshida [Phys. Plasmas **7**, 635 (2000)] are invoked and extended to derive scalings for the edge pedestal width and height with plasma parameters: these scalings come out in agreement with the established semiempirical scalings. The theory predictions are also compared with limited published H-mode data and the agreement is found to be very encouraging. © *2005 American Institute of Physics*. [DOI: 10.1063/1.1852468]

I. INTRODUCTION

When the heating power exceeds a critical value, the tokamak plasmas undergo a spontaneous self-organizing transition from a low (L-mode) to a high confinement state (H-mode).[1–3] The improved confinement is believed to be caused by the generation of a shear (zonal) flow, which is responsible for suppressing fluctuations and thus inhibiting transport. After this transition, a very steep pressure gradient develops at the edge. The height of the pressure pedestal is a natural figure of merit for energy confinement.[4] Elucidation of the physics of pedestal formation, and predicting its maximum achievable height are issues crucial for magnetic fusion devices.

A variety of theoretical models have been proposed to explain and predict experimentally established empirical scaling laws governing the pedestal width and height. Hubbard,[5] e.g., has provided a very comprehensive review of both the experiment and theory. Here it was pointed out that although the various theories have pedestal widths which are not very solidly in agreement with observations, the existence of a critical pressure gradient consistent with magnetohydrodynamics (MHD) stability limits seems to provide a reasonable quantitative comparison with observations. A careful comparison of empirical, semiempirical, and theory-based scalings of the pedestal height with the data (available in the pedestal database) was performed by Sugihara *et al.*[6] and Onjun *et al.*[7] The focus of the former study was to delineate the difference in scalings between plasmas with and without magnetic shear. Since the data subset with information on magnetic shear was limited, the study could not quite pin down the characteristic exponents associated with the relevant plasma parameters. In the study by Onjun *et al.*,[7] comparison of the pedestal height from a database comprising of over 500 shots from four tokamaks, with six different models showed that all the models had a root-mean-squared (rms) deviation which is in excess of 30%.

Thus, the present database studies, it seems, do not preferentially select any particular model or even a set of models. To understand the physics of the formation and the properties (including the maximum sustainable pressure) of the pedestal, therefore, a two-pronged attack is strongly indicated: a systematic buildup of the database as well as the development of pertinent theories.

In this paper, the theory of Mahajan and Yoshida[8] for the H-mode layer is extended to determine specifically the scalings of the pedestal height and width with plasma parameters. In a series of recent papers, Mahajan and Yoshida[9,10] have developed a theory of plasma relaxed states with flow. The centerpiece of this enterprise is the so-called double-Beltrami states (DB) obtained by the interaction of the magnetic and velocity fields. Under well-defined conditions,[8] the self-organized DB state provides a description for the edge region of the H-mode plasma. We will demonstrate that the detailed solution of the DB system with physically meaningful boundary conditions, augmented by the ballooning mode stability condition, determines uniquely the pedestal width and the pedestal height of the H-mode in tokamak plasmas. It is shown that the theoretically derived expressions for the height and width can be readily cast into forms that are equivalent to certain empirical scaling laws for DIII-D discharges.[11,12] Furthermore the theory will be compared with experimental observations from Japanese Atomic Energy Research Institute Tokamak-60 Upgrade (JT-60U) (Ref. 13) and Joint European Torus (JET) (Ref. 14).

II. EQUATIONS

The theoretical framework for this study is provided by the normalized two-fluid Hall MHD equations,

$$\frac{\partial n}{\partial t} + \nabla \cdot (n\mathbf{V}) = \mathbf{0}, \tag{1}$$

$$\frac{\partial \mathbf{A}}{\partial t} = \left(\mathbf{V} - \frac{\nabla \times \mathbf{B}}{n}\right) \times \mathbf{B} - \nabla \phi + \frac{\nabla p_e}{n}, \tag{2}$$

$$\frac{\partial}{\partial t}(\mathbf{V} + \mathbf{A}) = \mathbf{V} \times (\mathbf{B} + \nabla \times \mathbf{V}) - \nabla \left(\frac{V^2}{2} + \phi\right) - \frac{\nabla p_i}{n}. \tag{3}$$

Here, the magnetic field is normalized to B_0 whose magnitude is equal to the strength of the toroidal field in the edge region and the density is normalized to n_0, the density at the top of the density pedestal. In terms of B_0 and n_0, the following consistent normalizations emerge: the ion skin-depth λ_i for spatial variables, the Alfvén speed V_A for velocities, λ_i/V_A for time, $\lambda_i B_0$ for the vector potential $\mathbf{A}$, $\lambda_i B_0 V_A/c$ for the scalar potential ϕ, and $B_0^2/4\pi$ for the electron and ion pressures. At this stage, the plasma density is allowed to vary within the H-mode layer.

The detailed derivation of appropriate equations describing the H-mode layer is given in Ref. 8. For self-sufficiency of this paper, we provide here a brief summary. One begins by separating the total magnetic field into two parts: $\mathbf{B}=\mathbf{B}_0+\mathbf{B}_\mathbf{s}$, where B_0 represents the field rooted in currents outside the layer and B_s is the self-field generated by the currents in the layer. The curl of the Lorentz force due to be B_0 for each of the species can be expressed as a scalar potential to be determined *a posteriori*.[8] The fundamental basis of magnetic confinement, that the plasma pressure gradient in the edge will be supported by the diamagnetic pressure of the magnetic field, leads to the ordering $B_*/B_0=\beta/2$, B_* being the measure of the self-field.

The curl of Eqs. (2) and (3) yields the generalized vorticity equations,

$$\frac{\partial \mathbf{\Omega}_j}{\partial t} - \nabla \times (\mathbf{U}_j \times \mathbf{\Omega}_j) + (-1)^j \frac{1}{n^2} \nabla n \times \nabla p_j = \mathbf{0} \quad (j = 1,2) \tag{4}$$

with the two vorticities

$$\mathbf{\Omega}_1 = \mathbf{B}_s, \quad \mathbf{\Omega}_2 = \mathbf{B}_s + \nabla \times \mathbf{V} \tag{5}$$

and their associated generalized flows

$$\mathbf{U}_1 = \mathbf{V} - \frac{\nabla \times \mathbf{B}_s}{n}, \quad \mathbf{U}_2 = \mathbf{V}. \tag{6}$$

Here $p_1=p_e$ and $p_2=p_i$. For the full three-dimensional case, the last term vanishes for (1) n or T=constant and (2) $p_j=f_j(n)$, where $f_j(n)$ are general functions of the density n. For one-dimensional equilibrium, however, the last term is identically zero. Aligning the vorticities along the corresponding flows,

$$\mathbf{B}_s = \mu_1(n\mathbf{V} - \nabla \times \mathbf{B}_\mathbf{s}), \tag{7}$$

$$\mathbf{B}_\mathbf{s} + \nabla \times \mathbf{V} = \mu_2 n \mathbf{V}, \tag{8}$$

yields the double-Beltrami states. Here μ_1 and μ_2 are constants to be determined. In the steady state, these equations together with the Bernoulli condition and an equation of state define a fully self-consistent equilibrium. The Bernoulli condition to first order in β is

$$p + \mathbf{B}_s \cdot \mathbf{B}_0 = C. \tag{9}$$

Here $p=p_e+p_i$ and C is a constant. Finally, with an equation of state

$$\frac{p}{n^\gamma} = 1 \tag{10}$$

the set, namely, Eqs. (7)–(10), is complete. Incidentally the conservation of particle flux for the steady state in Eq. (1) is trivially satisfied. Thus for nonconstant density, these equations are the generalizations of Eqs. (12)–(14) of Ref. 8. Similar equations have been derived by Mahajan *et al.*[15] in the context of the solar atmosphere, where the flow and gravity determine the density in the generalized Bernoulli condition. For issues of accessibility, or the variational principles from which these states may be derived, the interested reader is directed to Refs. 8–10 and 16. The current goal is limited to using these solutions to make definitive predictions of plasma pedestal parameters in the H-mode layer.

III. NUMERICAL SOLUTIONS

In one-dimensional slab geometry, Eqs. (7)–(10) reduce to

$$\begin{aligned}
&\frac{dB_{s,y}}{dx} - nV_z + \frac{1}{\mu_1} B_{s,y} = 0,\\
&\frac{dB_{s,z}}{dx} + nV_y - \frac{1}{\mu_1} B_{s,y} = 0,\\
&\frac{dV_y}{dx} + B_{s,z} - \mu_2 n V_z = 0,\\
&\frac{dV_z}{dx} - B_{s,y} + \mu_2 n V_y = 0,\\
&n^{1/\gamma} + B_{s,z} = 0.
\end{aligned} \tag{11}$$

We have solved this system of equations numerically in the domain $0 \leqslant x \leqslant 1$, where $x=0$ is the inner boundary at the top of the pedestal, while $x=1$ is the outer boundary representing the last closed flux surface. The boundary conditions defining the layer are $V_y(0)=V_z(0)=B_{s,y}=0$, $B_{s,z}(0)=-1$. As pointed out by Mahajan and Yoshida,[8] with a requirement that the flows do not have any oscillations in the edge boundary layer and the specific boundary condition $B_{s,1}=0$, $\mu_1=1/\mu_2$. The eigenvalue μ_1 is adjusted to make the pressure go to zero at $x=1$. Four specific "equations of state" were employed: (1) constant density $n=1$, (2) isothermal with $\gamma=1$, (3) adiabatic with $\gamma=5/3$, and (4) adiabatic with $\gamma=3$; the last pertaining to a plasma with one degree of freedom which can be expected for a strongly magnetized plasma. In

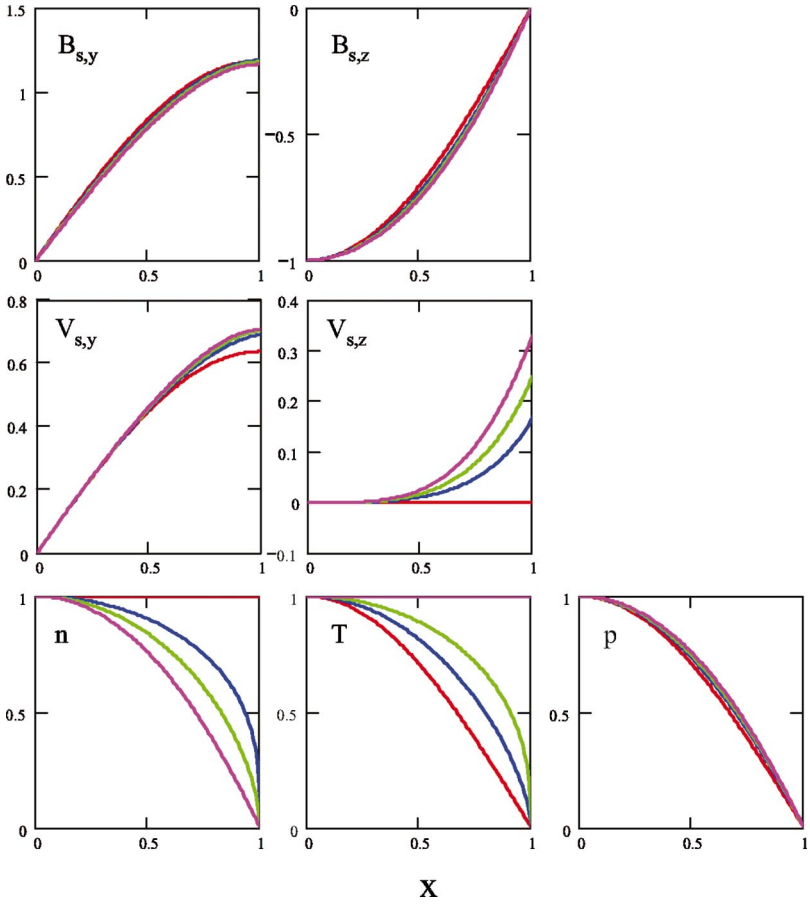

FIG. 1. (Color). $B_{s,y}$, $B_{s,z}$, $V_{s,y}$, $V_{s,z}$, n, T, p, vs x for constant density (red), $\gamma=1$ (magenta), $\gamma=5/3$ (green), and $\gamma=3$ (blue).

Fig. 1, are shown the equilibrium $B_{s,y}$, $B_{s,z}$, V_y, V_z, p, n, T, respectively, for the four different cases with the following color code: constant density (red), $\gamma=1$ (magenta), $\gamma=5/3$ (green), and $\gamma=3$ (blue). Three important conclusions may be drawn from the numerical work: (1) the total plasma pressure and the two magnetic field components are almost identical for all four cases, (2) the density, velocity and temperature profiles are significantly different for different equations of state, and (3) For the three nonconstant density examples, the equilibria have both poloidal as well as toroidal shear flows in the edge region. On examining the structure of the equations it is fairly clear that the flux $\mathbf{\Gamma}=n\mathbf{V}$, the magnetic field, and the pressure remain unchanged for different equations of state. The density and temperature profiles, however, change through the Bernoulli condition as the equation of state is changed. The velocity profile is automatically adjusted to preserve near invariance of the flux. It is important to note that density and temperature profiles for $\gamma=3$ look qualitatively similar to the experimentally observed profiles where for most tokamaks the density pedestal is steeper than the temperature pedestal. It is also apparent that a tangent hyperbolic fit to the density and temperature profiles can be reasonable, even though it was original motivated by a neutral penetration model.[17] The plasma current densities J_y and J_z and the radial electric field E_x are displayed as a function of x in Fig. 2 for the four cases shown in Fig. 1. The plasma develops a edge current on the scale of the ion skin depth. The radial electric field has been computed by assuming that the ion and electron temperatures are the same.

In this paper the principal goal is to determine the structure of the pressure pedestal. Since the pressure profile is mostly insensitive to the variation in density, we will, henceforth explore the constant density case for which analytical solutions already exist.[8] We will now derive the parametric scalings for the pressure pedestal characteristics by constraining the maximum pressure gradient by demanding stability to the ballooning mode.

IV. ANALYTICAL RESULTS

The general solution of the constant density DB system is known to be ($\nabla\times\mathbf{G}_{\Lambda_\pm}=\Lambda_\pm\mathbf{G}_{\Lambda_\pm}$),

$$\mathbf{V}=C_+\mathbf{G}_{\Lambda+}+C_-\mathbf{G}_{\Lambda-}, \tag{12}$$

$$\mathbf{B}_s=C_+(\mu_2-\Lambda_+)\mathbf{G}_{\Lambda+}+C_-(\mu_2-\Lambda_-)\mathbf{G}_{\Lambda-}, \tag{13}$$

with

$$\Lambda_\pm=\frac{1}{2}\left\{-\frac{1}{\mu_1}+\mu_2\mp\left[\left(\frac{1}{\mu_1}+\mu_2\right)^2-4\right]^{1/2}\right\}. \tag{14}$$

In one-dimensional slab geometry, it becomes

$$\mathbf{G}_{\Lambda\pm}=[0,\mathrm{Sin}(\Lambda_\pm x+\theta_\pm),\mathrm{Cos}(\Lambda_\pm x+\theta_\pm)]. \tag{15}$$

Using the same boundary conditions as in the numerical study discussed in the last section, the unnormalized solutions can be written as

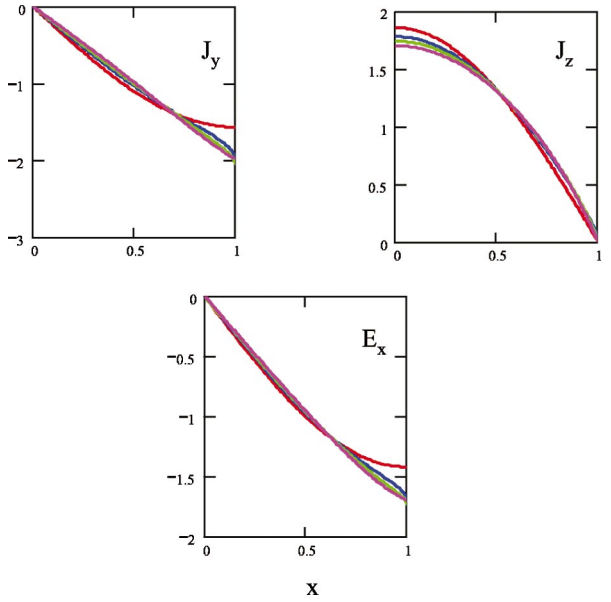

FIG. 2. (Color). $J_{s,y}$, $J_{s,z}$, $E_{s,x}$, vs x for constant density (red), $\gamma=1$ (magenta), $\gamma=5/3$ (green), and $\gamma=3$ (blue).

$$B_{s,z} = -B_* \cos\left(\frac{\pi x}{2\lambda_i}\right), \tag{16}$$

$$B_{s,y} = \left(1+\frac{4}{\pi^2}\right)^{1/2} B_* \sin\left(\frac{\pi x}{2\lambda_i}\right), \tag{17}$$

$$V_y = \frac{2}{\pi}\frac{B_*}{B_0} V_A \sin\left(\frac{\pi x}{2\lambda_i}\right). \tag{18}$$

The total pressure is related to the magnetic field by the pressure balance condition derived earlier

$$p + \frac{B_{s,z}B_0}{4\pi} = 0. \tag{19}$$

Furthermore, the plasma currents and the flow velocity $V_{E,y}$ due to radial electric field are also determined,

$$J_{s,y} = -\frac{cB_*}{8\lambda_i}\sin\left(\frac{\pi x}{2\lambda_i}\right), \tag{20}$$

$$J_{s,z} = \frac{cB_*}{8\lambda_i}\left(1+\frac{4}{\pi^2}\right)^{1/2}\cos\left(\frac{\pi x}{2\lambda_i}\right), \tag{21}$$

$$V_{E,y} = -\frac{2}{\pi}\left(1+\frac{\pi^2\tau}{4(1+\tau)}\right)\frac{B_*}{B_0}V_A \sin\left(\frac{\pi x}{2\lambda_i}\right). \tag{22}$$

Equations (16)–(22) form an explicit and complete solution except for a single undetermined quantity; the magnitude B_* of the magnetic field or equivalently the plasma pressure at the top of the pedestal. To determine this it is stipulated that the H-mode state maximizes the pressure gradient consistent with the ballooning stability criterion,

$$\frac{8\pi q^2 R}{B_0^2}\frac{dp}{dx} = \alpha_c, \tag{23}$$

where q is the local plasma safety factor R, the major radius and the parameter α_c contains the plasma shaping effects[7] in determining the stability of these modes. The pressure pedestal height expressed as pedestal β, then, is

$$\beta_{ped} = \frac{2\alpha_c}{\pi}\frac{\lambda_i}{q^2 R} = 2\frac{B_*}{B_0} \tag{24}$$

with the pedestal width given by

$$\Delta_{ped} = \lambda_i. \tag{25}$$

Since the amplitudes of all the physical quantities defined in Eqs. (16)–(22) are determined by B_*, the stability criterion which determines the maximum pedestal β, determines the magnitude of B_* [Eq. (24)] and hence the magnitude of all these physical quantities. A comparison of these quantities with experimental data for some typical parameters will be presented at the end of this section. However, first, to conform to the standard practice of expressing the empirical scalings in terms of the poloidal Larmor radius ρ_{pi}, and recalling that $\lambda_i = \sqrt{2}\rho_{pi}/\sqrt{\beta_{pi}}$, where β_{pi} is the ion poloidal plasma β, we convert Eqs. (21) and (22) to the alternative form

$$\beta_{ped} = \frac{2}{q^2}\left(\frac{\alpha_c}{\pi}\right)^{2/3}\left(1+\frac{T_e}{T_i}\right)^{1/3}\left(\frac{\rho_{pi}\epsilon}{R}\right)^{2/3} \tag{26}$$

and the pedestal width as

$$\frac{\Delta_{ped}}{R} = \left(\frac{\pi}{\alpha_c}\right)^{1/3}\left(1+\frac{T_e}{T_i}\right)^{1/3}\left(\frac{\rho_{pi}\epsilon}{R}\right)^{2/3}. \tag{27}$$

Here $\epsilon = a/R$ is the inverse aspect ratio. In this form, the theoretical prediction for the pedestal width closely resembles one of the empirical scalings for data from DIII-D.[12] The earliest theories on L-H transitions invoking ion banana orbit loss[18,19] implied that the pedestal width should scale as the poloidal larmor radius ρ_{pi} and this has guided subsequent comparisons with observations.[20] It is clear that a convincing comparison with data requires a more focused effort which is being actively pursued. Nevertheless, there are many features of the scalings derived above which reflect consistency with observations on DIII-D, JT-60U, and JET.

Before we end this section we give quantitative estimates of various quantities to show that they are in the range

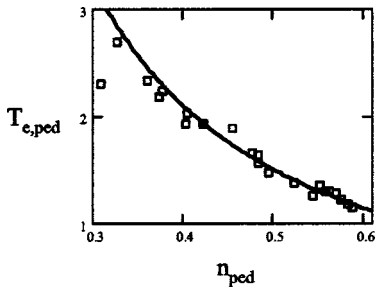

FIG. 3. $T_{e,ped}$ for experimental points (squares) and theory (solid line) vs n_{ped} for JET discharges.

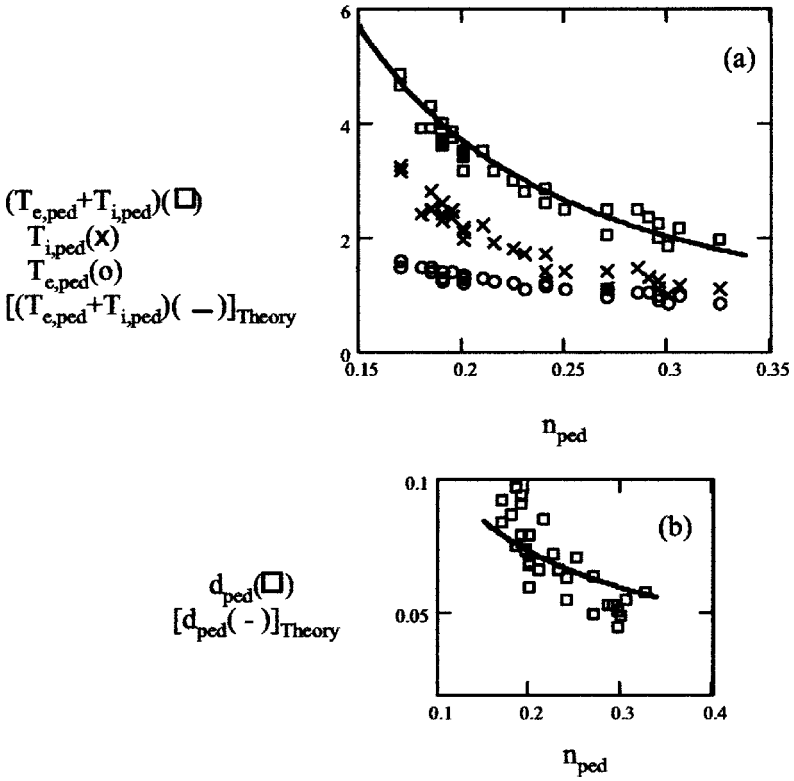

FIG. 4. (a) Experimental $T_{e,ped}$ (circle), $T_{i,ped}$ (cross), $T_{e,ped}+T_{i,ped}$ (square), theory $T_{e,ped}+T_{i,ped}$ (solid line) vs n_{ped} for JT-60U discharges. (b) Experimental pressure pedestal width d_{ped} (square) and theoretical pedestal width (solid line) vs the pedestal density n_{ped}.

of measurements on present-day machines. We find that for pedestal densities varying from $10^{13}-5\times10^{14}$ cm^{-3}, the pressure pedestal width varies from 10.3 to 1.5 cm. For the toroidal field $B_0=2$ T, $A_H=2$, $Z=1$, $\alpha_c=3-6$, $n_{ped}=3\times10^{13}$ cm^{-3}, $q=3$, and $R=2$ m, the sum of the electron and ion temperatures at the top of the pedestal, $T_{e,ped}+T_{i,ped}=2-4$ keV. The Hall current densities $J_{s,y}\sim J_{s,z}=30$ A/cm^2, are comparable to the Bootstrap current using the Sauter formula[21] and the $E\times B$ flow velocity $V_{E,y}=12$ km/s.

V. COMPARISON WITH OBSERVATIONS

We first discuss qualitatively our results in the context of general observations on pedestals and their scaling on DIII-D and JT-60U, and then make quantitative comparisons with specific data on these machines as well as on JET. In its most basic form, the height and the width of the pressure pedestal scale as the ion skin-depth [(24) and (25)]. It was shown by Osborne *et al.*[22] for DIII-D [see Fig. 1(b) of Osborne *et al.*], that for different triangularities, the quantity $P_{e,ped}R^2/I_p^2$, decreased as a function of $n_{e,ped}$, and the highest pedestal heights occur for the highest triangularity. Here $P_{e,ped}$ is the electron pressure at the top of its pedestal, $n_{e,ped}$ is the electron density at the pedestal height, R is the major radius, and I_p is the plasma current. The experimental results, cited above, agree with Eq. (21) on two counts. First, the decrease in the pedestal height with density is consistent with the inverse dependence on the square root of the density of the ion skin depth. Second, the observed dependence on triangularity is to be expected from the plasma shape parametric dependence of α_c.[7] In fact the observed decrease in the pedestal height at high density[22] is attributed to the decrease in the pedestal width—a deduction fully consistent with the present theory. The scaling implied by the alternate form [Eq. (23)], in fact, agree very well with the best-fit empirical scaling for DIII-D.[12] The slightly weaker ρ_{pi} is in reasonable agreement with the linear scaling of the pedestal width observed on JT-60U for edge-localized-mode-free H-mode discharges.[20] In fact, in a study comparing JT-60U and DIII-D, Hatae *et al.*[23] investigated the pedestal width (Δ) scaling $\Delta/R\propto(\rho_{pi}/R)^{0.66}$, and found it to be in good agreement with both the devices. However, they concluded that the normalized width should have some aspect ratio dependence. Equation (24), which has the same ρ_{pi} dependence used in the comparative study, also has a dependence on the inverse aspect ratio ϵ which can be tested against the data.

Next we make quantitative comparisons of the pedestal height and width (if available) with two machines using data in published literature. To facilitate comparison, we cast the pedestal width and pedestal height into practical units. In meters, the pedestal width is given by

$$\Delta(m)=\frac{0.023}{Z}\left(\frac{A_H}{n_{ped}}\right)^{1/2} \tag{28}$$

and the sum of the ion and electron temperatures (in keV) is

$$T_{e,ped}+T_{i,ped}=0.36\frac{\alpha_c A_H^{1/2}B_T^2}{Zq^2Rn_{ped}^{3/2}}. \tag{29}$$

In these formulas, the density has been normalized to $10^{20}/\mathrm{m}^3$, the major radius is in meters, the magnetic field is in Tesla, Z is the ionic charge, and A_H is the ion atomic mass relative to hydrogen. The first comparison is with the data from JET drawn[24,25] from fifteen discharges with high elongation and triangularity and $I_P=2.5$ MA and $B_T=2.3$ T. All these discharges displayed type I ELMy behavior. In Fig. 3,

the square boxes are experimental data points. Since the dataset does not include the ion temperature, we have assumed that the electron and ion temperatures are equal. This is expected to be true for the high density discharges but not so for the lower density cases. The solid line is a plot of Eq. (29) and fits the data for $\alpha_c/q^2=0.9$. If $q=2.8$ at the top of the pedestal, then the fit requires $\alpha_c=7$. This is consistent with ballooning mode stability studies which indicate that for low elongation and triangularity, $\alpha_c=3$, while for high elongation and triangularity $\alpha_c=6-8$.[26,27]

In Figs. 4(a) and 4(b), the data from JT-60U is compared[28] with the theory. For these type I ELMing discharges, with low elongation and triangularity, $I_p=1.8$ MA and $B_T=3$ T. In Figure 4(a) the temperature at the top of the pedestal is plotted as a function of the pedestal density. The circles (crosses) represent the measured electron (ion) temperature. The boxes are the sum of the experimental ion and electron temperatures at the top of the pedestal. The solid curve is from Eq. (29) with $\alpha_c/q^2=0.22$. If we assume that $q=3.5$ at the pedestal height, then $\alpha_c=2.7$ which is the low value expected for these low elongation and low triangularity discharges. What is clearly seen from the data is that the electron and ion temperatures at the top of the pedestal are equilibrated for the high density discharges but not for the low density ones. Plotted in Fig. 4(b) are the experimental pedestal widths (boxes), the theoretical pedestal widths (solid line) given by Eq. (28).

The agreement between the data and the theoretical predictions is reasonably good. We remind the reader that in all these comparisons we have tacitly assumed that α_c/q^2 is the same for all discharges for a given device. This is, to some degree, justified because for the shots used in these studies, the plasma current, magnetic field, elongation, and triangularity were nearly constant or varied in a narrow range. However, for a more reliable comparison one should compute α_c/q^2 from a stability code and use it in Eq. (29) for each discharge.

VI. CONCLUSIONS

In conclusion, the theory of Mahajan and Yoshida[8] together with the constraint on the pressure gradient dictated by ballooning modes stability, predicts fully determined expressions for the width and height of the pressure pedestal for an H-mode plasma. For a realistic equation of state ($\gamma=3$), the theory yields a steeper density profile compared to the temperature profile consistent with the profiles observed inside the closed flux region at the edge of most tokamaks. The sign of the electric field associated with the flow is also consistent with experiment (inward directed). For all nonconstant density cases, a finite toroidal flow is predicted. Equation (27) also agrees with one of the empirical scalings found earlier for data from DIII-D.[12] With the existing error bars on data, however, some other empirical scalings also do as well as the class represented by Eq. (27). The principal merit of the current effort is that a physics-based self-organization model has been harnessed to derive the results. A more quantitative, though limited, comparison of the theory with experimental data involving density scans for JET, JT-60U, and DIII-D as shown in Figs. 3 and 4, respectively, yields encouraging agreement. Naturally a much more thorough and detailed comparison with data from various machines, with systematic scan of plasma parameters, is needed. Extension of the theory to two dimensions is planned for the near future.

ACKNOWLEDGMENTS

The authors would like to thank T. Onjun and the Lehigh group for discussions related to their work. They would also like to thank Dr. Urano and Dr. Kamada for providing them with the data for JT-60U used in Fig. 4 and Dr. Sugihara for providing the data for Fig. 3. The work of PNG was supported by the U.S. Department of Energy under Grant No. DE-FG02-93ER54197 at UMD. The study of SMM was supported by U.S. Department of Energy Contract No. DE-FG03-96ER-54366.

[1] ASDEX Team and F. Wagner, Phys. Rev. Lett. **49**, 1408 (1982).
[2] DIII-D Team and K. H. Burrell, Plasma Phys. Controlled Fusion **34**, 1859 (1992).
[3] R. J. Groebner, Phys. Fluids B **5**, 2343 (1993).
[4] M. Kotschenreuther, W. Dorland, Q. P. Liu, G. M. Hammett, M. A. Beer, S. A. Smith, A. Bondeson, and S. C. Cowley, in *Proceedings of the 16th Conference Plasma Physics Contrl Fusion Research Montreal, 1996* (IAEA, Vienna, 1997), Vol. 2, p. 371.
[5] A. Hubbard, Plasma Phys. Controlled Fusion **42**, A15 (2000).
[6] International H-Mode Edge Pedestal Expert Group, M. Sugihara, and T. Takizuka, Plasma Phys. Controlled Fusion **44**, A299 (2002).
[7] T. Onjun, G. Bateman, A. H. Kritz, and G. Hammett, Phys. Plasmas **9**, 5018 (2002).
[8] S. M. Mahajan and Z. Yoshida, Phys. Plasmas **7**, 635 (2000).
[9] S. M. Mahajan and Z. Yoshida, Phys. Rev. Lett. **81**, 4863 (1998).
[10] Z. Yoshida and S. M. Mahajan, Phys. Rev. Lett. **88**, 095001 (2002).
[11] J. L. Luxon, Nucl. Fusion **42**, 614 (2002).
[12] T. H. Osborne, K. H. Burrell, R. J. Groebner, L. L. Lao, A. W. Leonard, R. Maingi, R. L. Miller, G. D. Porter, G. M. Staebler, and A. D. Turnbull, J. Nucl. Mater. **266–269**, 131 (1999).
[13] JT-60 Team and S. Ishida, Nucl. Fusion **39**, 1211 (1999).
[14] G. J. Sadler, S. W. Conroy, O. N. Jarvis *et al.*, Fusion Technol. **18**, 556 (1990).
[15] S. M. Mahajan, K. I. Nikol'skaya, N. Shatashvili, and Z. Yoshida, Astrophys. J. **576**, L161 (2002).
[16] Z. Yoshida and S. M. Mahajan, J. Math. Phys. **40**, 5080 (1999).
[17] R. J. Groebner, M. A. Mahdavi, A. W. Leonard, T. H. Osborne, and G. D. Porter, Plasma Phys. Controlled Fusion **44**, A265 (2002).
[18] S.-I. Itoh and K. Itoh, Phys. Rev. Lett. **60**, 2276 (1988).
[19] K. C. Shaing and E. C. Crume, Phys. Rev. Lett. **63**, 2369 (1989).
[20] T. Hatae, Y. Kamada, S. Ishida, T. Fukuda, T. Takizuka, H. Shirai, Y. Koide, M. Kikuchi, H. Yoshida, and O. Naito, Plasma Phys. Controlled Fusion **40**, 1073 (1998).
[21] P. B. Snyder (private communication).
[22] DIII-D Team and T. H. Osborne, J. R. Ferron, R. J. Groebner, L. L. Lao, A. W. Leonard, M. A. Mahdavi, P. B. Snyder, and the , in *Proceedings of the 29th EPS Conference Plasma Physics and Controlled Fusion, Montreaux,* edited by R. Behn and C. Varandas (European Physical Society, Mulhouse, 2002), ECA Vol. 26B, p. P1.062.
[23] T. Hatae, T. H. Osborne, Y. Kamada, R. J. Groebner, T. Takizuka, T. Fukuda, and L. L. Lao, Plasma Phys. Controlled Fusion **42**, A283 (2000).
[24] M. Sugihara, Yu. Igitkhanov, G. Janeschitz, A. E. Hubbard, Y. Kamada, J. Lingertat, T. H. Osborne, and W. Suttrop, Nucl. Fusion **40**, 1743 (2000).
[25] J. Lingertat, V. Bhatnagar, G. D. Conway, I.-G. Eriksson, K. Günther, M. von Hellermann, M. Mantsinen, V. Parail, R. Prentice, G. Saibene, R. Smith, and K.-D. Zastrow, J. Nucl. Mater. **266–269**, 124 (1999).
[26] T. Onjun (private communication).
[27] P. B. Snyder, H. R. Wilson, J. F. Ferron, L. L. Lao, A. W. Leonard, D. Mossessian, T. H. Osborne, A. D. Turnbull, and X. Q. Xu, Nucl. Fusion **44**, 320 (2004).
[28] H. Urano, Y. Kamada, H. Shirai, T. Takizuka, S. Ide, T. Fujita, and T. Fukuda, Nucl. Fusion **42**, 76 (2002).